Journal of Solid State Chemistry 184 (2011) 1186–1194

Contents lists available at ScienceDirect

Journal of Solid State Chemistry

journal homepage: www.elsevier.com/locate/jssc

Thermodynamic studies on lithium ferrites

S.K. Rakshit [a,*], S.C. Parida [a], Y.P. Naik [a], Ziley Singh Chaudhary [a], V. Venugopal [b]

[a] Product Development Division, Bhabha Atomic Research Centre, Trombay, Mumbai 400 085, India
[b] Radiochemistry & Isotope Group, Bhabha Atomic Research Centre, Trombay, Mumbai 400 085, India

ARTICLE INFO

Article history:
Received 20 December 2010
Received in revised form
12 March 2011
Accepted 16 March 2011
Available online 21 March 2011

Keywords:
Lithium ferrite
Differential scanning calorimetry
Knudsen effusion mass spectrometry
Thermodynamic properties

ABSTRACT

Thermodynamic studies on ternary oxides of Li–Fe–O systems were carried out using differential scanning calorimetry, Knudsen effusion mass spectrometry, and solid-state electrochemical technique based on fluoride electrolyte. Heat capacities of $LiFe_5O_8$(s) and $LiFeO_2$(s) were determined in the temperature range 127–861 K using differential scanning calorimetry. Gibbs energies of formation of $LiFe_5O_8$(s) and $LiFeO_2$(s) were determined using Knudsen effusion mass spectrometry and solid-state galvanic cell technique. The combined least squares fits can be represented as

$$\Delta_f G^o_m(LiFe_5O_8,s,T)/kJ\ mol^{-1}\ (\pm 6) = -2341 + 0.6764(T/K) \quad (588 \le T/K \le 971)$$

$$\Delta_f G^o_m(LiFeO_2,s,T)/kJ\ mol^{-1}\ (\pm 3) = -708 + 0.1656(T/K) \quad (569 \le T/K \le 1021)$$

The temperature independent term of the above equations represents $\Delta_f H^o_m(T_{av})$ and temperature dependent term represents negative change in entropy of the respective compounds. Thermodynamic analysis shows that $LiFe_5O_8$(s) is more stable compared to $LiFeO_2$(s).

1. Introduction

Ternary oxides, $LiFe_5O_8$(s) and $LiFeO_2$(s) of Li–Fe–O system are of considerable interest due to their several technological applications. $LiFeO_2$(s) is used as electrode in rechargeable lithium batteries due to its low cost and less toxicity [1–3]. $LiFe_5O_8$(s) is ferrimagnetic in nature and used in the microwave field and in memory core due to its square hysteresis loop, high saturation magnetization and high Curie temperature [4]. Lithium ferrites have also been developed as a replacement for yttrium iron garnet (YIG) due to their low cost [5]. A large number of literatures have been published on different synthesis routes, electrical and magnetic properties of lithium ferrites [6–10]. Due to their chemical and thermal stabilities as well as less radiation damage, lithium based oxides are also considered as suitable candidates for solid breeder materials in the irradiation blanket of future *D–T* fusion nuclear reactor. These materials, on neutron irradiation, produce tritium in appreciable quantity which then acts as a fuel component of the reactor. Thermal properties such as heat capacity will play a major role in designing of the blanket system which is responsible for efficient transfer of heat generated by nuclear fusion reaction to the coolant [11,12]. Several authors have reported the thermodynamic data for Li–Fe–O system [13–17]. However, there are large deviations among them.

In this study, α-$LiFe_5O_8$(s) and α-$LiFeO_2$(s) were prepared using solid-state reaction route and thermodynamic studies were carried out using differential scanning calorimetry (DSC), Knudsen effusion quadrupole mass spectrometry (KEQMS) and solid-state galvanic cell technique. The thermodynamic data will be compared with that available in literature.

2. Experimental

2.1. Synthesis of lithium ferrites

$LiFe_5O_8$(s) and $LiFeO_2$(s) were prepared by taking suitable stoichiometric ratios of preheated Li_2CO_3(s) and Fe_2O_3(s) (LEICO Ind. Inc., mass fraction 0.9999) in molar ratios of (1:5) and (1:1), respectively. Powders of individual compounds were first mixed

* Corresponding author. Fax: +91 22 25505151.
E-mail addresses: swarup_kr@rediffmail.com, swarupkr@barc.gov.in (S.K. Rakshit).

0022-4596/$ - see front matter © 2011 Elsevier Inc. All rights reserved.
doi:10.1016/j.jssc.2011.03.033

homogenously in an agate mortar and pestle and compacted into pellets using a tungsten carbide lined steel die at a pressure of 20 MPa. The pellets were initially heated at 900 K for 50 h in air in a re-crystallized alumina boat. The pellets were then cooled and re-ground to powder and then re-pelletized and heated at 1150 K for 48 h. The resultant samples were then characterized by X-ray powder diffraction (XRD) technique using a table top powder diffractometer (GBC, EMMA, Australia) with Cu-$K\alpha$ radiation at $\lambda = 1.54056$ Å and found to be pure phases of α-$LiFe_5O_8$(s) and α-$LiFeO_2$(s). The powder XRD patterns of both the compounds are given in Fig. 1.

Powder samples of $LiFe_5O_8$(s) and $LiFeO_2$(s) were used for DSC studies. Phase mixtures {$2LiFe_5O_8$(s)+Li_2CO_3(s)+$5Fe_2O_3$(s)} and {$2LiFeO_2$(s)+Li_2CO_3(s)+Fe_2O_3(s)} were prepared for KEQMS experiment by homogeneously mixing the individual compounds and pelletized using a tungsten carbide lined steel die and then sintered at 600 K for 24 h under high vacuum.

The phase mixtures of {$2LiFe_5O_8$(s)+2LiF(s)+$5Fe_2O_3$(s)} and {$5LiFeO_2$(s)+$LiFe_5O_8$(s)+4LiF(s)} were prepared on the basis of phase relations in the Li_2O–Fe_2O_3 pseudo-binary system. The pellets were sintered at 800 K for 24 h in high purity oxygen atmosphere devoid of moisture and hydrogen. These pellets were then used for solid-state galvanic cell studies.

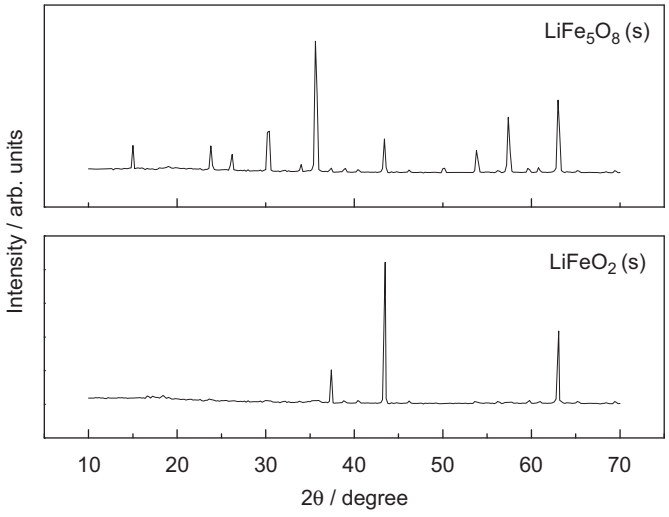

Fig. 1. Powder XRD patterns of $LiFe_5O_8$(s) and $LiFeO_2$(s).

2.2. Measurement of heat capacity using differential scanning calorimetry

Heat capacity measurements were carried out using a heat-flux type DSC. (Model: DSC131, Setaram Instrumentation, France). The temperature and the energy calibrations and the methods of heat capacity measurements are described in details by Rakshit et al. [18]. In order to check the accuracy of the heat capacity measurements, heat capacity of Fe_2O_3 (mass fraction: 0.9999. Alfa Aesar, USA) was measured. The values of heat capacity of Fe_2O_3 were found to be within $\pm 2\%$ compared to the literature values [19].

2.3. Knudsen effusion quadrupole mass spectrometry

The Knudsen effusion mass spectrometric technique is very useful for carrying out high temperature thermodynamic studies. Generally, traditional magnetic sector mass spectrometer attached to Knudsen effusion system is preferable among other type of mass spectrometers. Murray et al. [20] have shown that thermodynamic data obtained by Knudsen effusion technique using magnetic sector spectrometer and quadrupole mass spectrometer are in good agreement for pure chromium and chromium-silicon samples. However, quadrupole mass spectrometer has no significant advantages over magnetic mass spectrometer but they are very compact and relatively inexpensive. Stolyarova et al. [21] have reported that quadrupole mass spectrometer coupled to Knudsen cell can effectively be used for thermodynamic studies at high temperatures.

In this study, a Residual Gas Analyzer (RGA) coupled to Knudsen effusion system was used for equilibrium partial pressure measurements. An RGA is a quadrupole mass spectrometer in which the ionizer is immersed in the gas to be analyzed, and the ionizer is characterized by an open construction in which the gas may enter and leave in all directions. It is assumed that the gas is homogeneous and that changes in the gas density with time occur slowly enough such that the instrument is always in equilibrium with the gas. This instrument can be used to identify

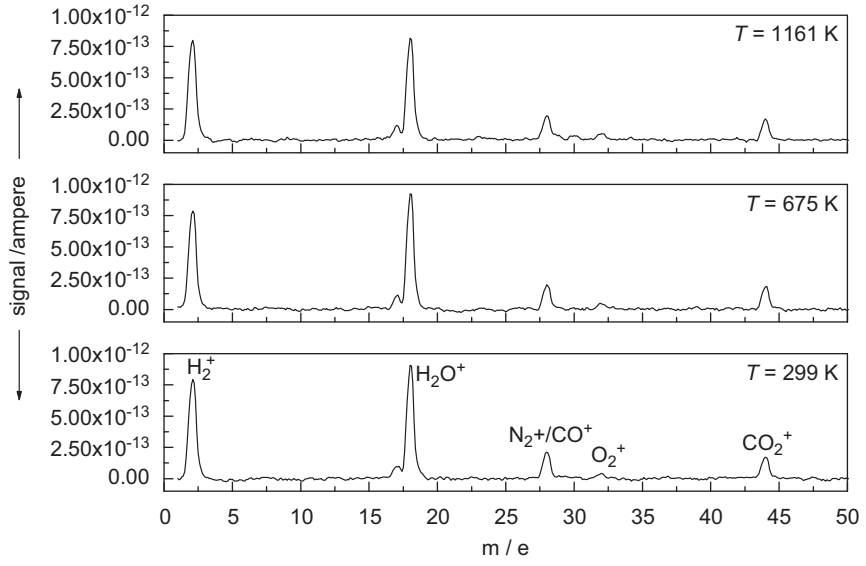

Fig. 2. Background mass spectrum of empty Knudsen cell as a function of temperature.

the kind of molecules present in the gaseous phase and, when calibrated, can be used to determine concentrations or partial pressures [22–24] of individual species. The experimental setup, mass spectrometric parameter and the calibration experiments are explained in detail by Rakshit et al. [25].

2.3.1. Partial pressure measurements of $CO_2(g)$ over equilibrium phase mixtures using KEQMS technique

Prior to actual experiment, the background signals were monitored by heating the Knudsen chamber with empty Knudsen cell at different temperatures from ambient to 1161 K at pressure level $\sim 1\times10^{-5}$ Pa. The background signals as a function of temperature are shown in Fig. 2. It is evident from the figure that the background signals corresponding to H_2^+, N_2^+, CO^+ and CO_2^+ do not change appreciably with change in temperature. During experiments, the actual signals were obtained by subtracting the ion intensities due to background.

The Knudsen cell used was made of 15 mol% calcia stabilized zirconia (CSZ) with a thin cylindrical orifice of diameter 0.8 mm and height 0.2 mm at the center of the lid. The detected ion signal (I_i^+) measured using a Faraday cup detector is related to the partial pressure of the vapor species (p_i) by

$$p_i = K_{\text{inst}} I_i^+ T/(\sigma_i a_i) \quad (1)$$

where K_{inst} is the instrumental constant, I_i^+ is the measured ion current in ampere, T is the absolute temperature near the Knudsen cell, σ_i is the electron impact cross-section and a_i isotopic abundance of the specific ion. Eq. (1) can be represented as

$$\ln p_i = \ln K_{\text{inst}} + \ln(I_i^+ T) - \ln\sigma_i - \ln a_i \quad (2)$$

Eq. (2) is used to calculate the instrument constant (K_{inst}) by calibrating with a standard having known partial pressures at different temperatures.

Huang et al. [26] have reported the thermodynamic data of $Na_4Fe_6O_{11}(s)$ by measuring the partial pressure of $CO_2(g)$ over $\{2Na_2CO_3(s)+3Fe_2O_3(s)\}$ phase mixture using Knudsen effusion mass spectrometry from 918 to 1013 K. Similar approach was adopted in this study to determine the Gibbs energies of formation of $LiFe_5O_8(s)$ and $LiFeO_2(s)$ by measuring the partial pressure of $CO_2(g)$ over the equilibrium phase mixtures of $\{LiFe_5O_8(s)+Li_2CO_3(s)+5Fe_2O_3(s)\}$ and $\{2LiFeO_2(s)+Li_2CO_3(s)+Fe_2O_3(s)\}$, respectively.

The ion intensities of CO_2^+ over these equilibrium phase mixtures were measured using KEQMS. For each measurement, two sets of experiments were carried out and the ion intensities for other gaseous species were in background level during the measurement. Subsequently, partial pressures of carbon dioxide, $p(CO_2)$ over the phase mixture were obtained using Eq. (2). After the mass spectrometric measurements, the resultant phase mixtures were analyzed by X-ray powder diffraction technique and found to be the mixture of corresponding lithium ferrite, Li_2CO_3 and Fe_2O_3. Therefore, it was assumed that the following equilibrium reactions were established inside the Knudsen cell under experimental conditions:

$$Li_2CO_3(s)+5Fe_2O_3(s) = 2LiFe_5O_8(s)+CO_2(g) \quad (3)$$

$$Li_2CO_3(s)+Fe_2O_3(s) = 2\,LiFeO_2(s)+CO_2(g) \quad (4)$$

Therefore, the measured $p(CO_2)$ corresponds to the equilibrium partial pressures of $CO_2(g)$ for above reactions.

2.4. Solid-state galvanic cell technique with CaF_2 electrolyte

The experimental setup and the cell assembly used in this study have been explained in detail by Rakshit et al. [25]. A schematic diagram of the fluoride cell used in this experiment is shown in Fig. 3. Optical grade single crystal of $CaF_2(s)$ pellet of 6 mm diameter and 3 mm thickness (supplied by Solon Technologies, Inc., USA) was used as fluoride ion conducting electrolyte. It is a single compartment cell with provisions for passing purified oxygen gas during the experiment and to measure the temperature of the cell near the electrode/electrolyte interface. High purity oxygen gas at one atmospheric pressure was allowed to pass through successive traps of silica gels, molecular sieves, oxidized form of BTS catalyst and anhydrous magnesium perchlorate for removal of traces of $H_2(g)$ and moisture. The reference electrode, the electrolyte and the sample electrode stacked one over the other were kept in the isothermal temperature zone of a Kanthal wire wound furnace. The furnace temperature was controlled within ± 1 K using a PID temperature controller. The cell was first standardized using phase mixtures of $\{CaO(s)+CaF_2(s)\}$ and $\{MgO(s)+MgF_2(s)\}$ as two standard electrodes.

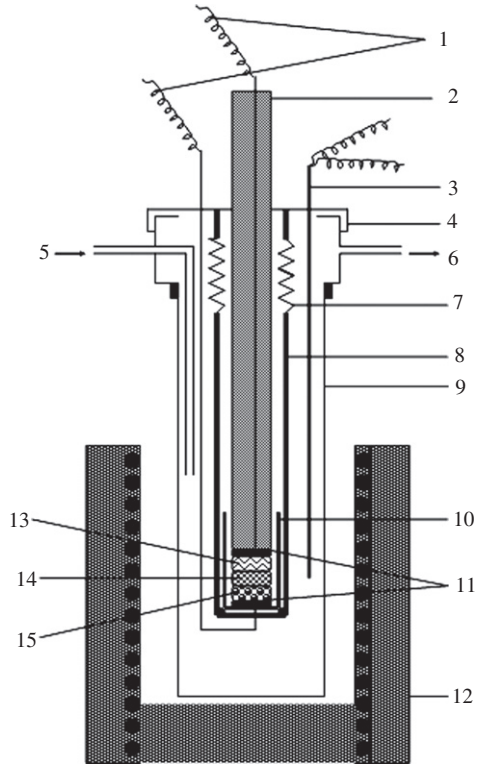

Fig. 3. Schematic diagram of solid-state electrochemical cell based on fluoride electrolyte. 1—Pt lead wires; 2—alumina pressing tube; 3—thermocouple; 4—stainless steel flange; 5—gas inlet; 6—gas outlet; 7—spring; 8, 9: quartz tube; 10—alumina cup; 11—Pt disks; 12—Kanthal wire wound furnace; 13—reference electrode; 14—$CaF_2(s)$ electrolyte; 15—sample electrode.

The cell can be represented as

$$\text{Cell (1)}: (-)\text{Pt}, O_2(g)/\{CaO(s)+CaF_2(s)\}//CaF_2(s) //\{MgO(s)+MgF_2(s)\}/O_2(g), \text{Pt}(+)$$

After standardization, the reversible emf's of the following solid-state galvanic cells were measured as a function of temperature

$$\text{Cell (2)}: (-)\text{Pt}, O_2(g)/\{CaO(s)+CaF_2(s)\}//CaF_2(s) //\{LiFe_5O_8(s)+Fe_2O_3(s)+LiF(s)\}/O_2(g), \text{Pt}(+);$$

$$\text{Cell (3)}: (-)\text{Pt}, O_2(g)/\{CaO(s)+CaF_2(s)\}//CaF_2(s) //\{LiFeO_2(s)+LiFe_5O_8(s)+LiF(s)\}/O_2(g), \text{Pt}(+)$$

The cell temperature close to the electrodes was measured using a pre-calibrated (ITS-90) chromel–alumel thermocouple. The cell e.m.f. (± 0.2 mV) was measured using a Keithley 614

electrometer (input impedance $>10^{14}\,\Omega$). At low temperatures, stable values of emf were obtained approximately after 72 h whereas at successive higher temperatures, stability in emf values was observed within 5–6 h. The reversibility of the solid-state electrochemical cells was evaluated by micro-coulometric titration in both directions. The electrode pellets after the emf measurements were re-examined by XRD analysis and the phase compositions were found unchanged.

3. Results and discussions

3.1. Heat capacity measurements of $LiFe_5O_8$(s) and $LiFeO_2$(s)

The isobaric molar heat capacities ($C^{o}_{p\,m}$) of $LiFe_5O_8$(s) and $LiFeO_2$(s) were measured as a function of temperature from (i) 127–308 K and (ii) 308–861 K. The variation of heat capacities of these ternary oxides were plotted as a function of temperature and shown in Fig. 4. The individual values of heat capacities were least square fitted as a function of temperature in low and high temperature ranges and the best fits are represented as

(i) 127–308 K

$$C^{o}_{p,m}(LiFe_5O_8)\,JK^{-1}\,mol^{-1} = -1404.88307 + 26.1312\,(T/K) - 0.16081\,(T/K)^2 + 4.4688\times10^{-4}\,(T/K)^3 - 4.6045210^{-7}\,(T/K)^4$$

$$C^{o}_{p,m}(LiFeO_2)\,JK^{-1}\,mol^{-1} = 47.62148 - 0.81106\,(T/K) + 0.005\,(T/K)^2 - 2.92974\times10^{-6}\,(T/\,K)^3 - 1.18764\times10^{-8}\,(T/K)^4$$

(ii) 296–861 K

$$C^{o}_{p,m}(LiFe_5O_8)\;JK^{-1}\,mol^{-1} = 253.1 + 0.2479(T/K) - 2571970/(T/K)^2$$

$$C^{o}_{p,m}(LiFeO_2)\,JK^{-1}\,mol^{-1} = 102.5 + 0.0281(T/K) - 2823190/(T/K)^2$$

Heat capacities of $LiFeO_2$(s) are reported by King [17] and Barin [27], which has been compared with that of our study in Fig. 4. The figure shows that heat capacity values are in close agreement with that of literature [17,27] at temperatures above 298 K whereas the low temperature (<298 K) values of this study are lower than King's value [17] by as much as 50%. This large difference in heat capacity values may be due to the two different techniques used for measurement. Heat capacities of $LiFe_5O_8$(s) are not reported by any researchers and the data presented in this study are first time data.

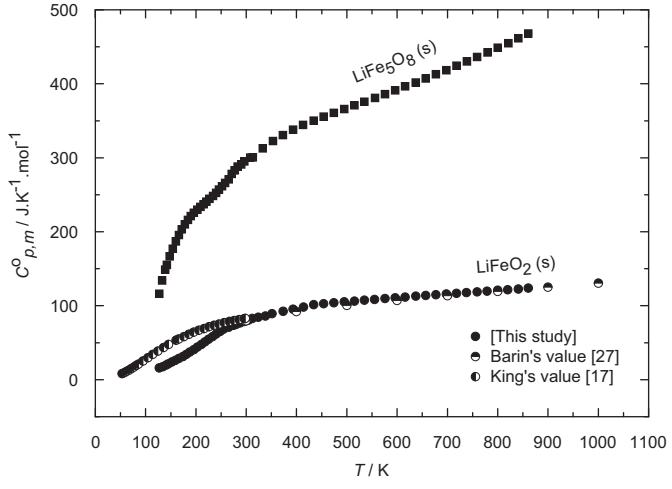

Fig. 4. Molar heat capacities of $LiFe_5O_8$(s) and $LiFeO_2$(s) as a function of temperature.

3.2. Partial pressure measurements over ternary phase mixtures using KEQMS

Prior to the actual experiment, the KEQMS apparatus was first calibrated by measuring the ion intensities of CO_2^+ as a function of temperature over different equilibrium phase mixtures whose partial pressure of CO_2(g) is known from the literature. For permanent gaseous species such as CO_2, $\ln\sigma = -45.52$ at 30 eV [28] and isotopic abundance is 100%, hence, Eq. (2) can be expressed as

$$\ln p_i = \ln K_{inst} + \ln(I_i^+ T) + 45.52 \quad (\text{for } i = CO_2) \tag{5}$$

The detail of the calibration is explained by Rakshit et al. [25]. The calibration constant calculated at 30 eV for $\{Li_2CO_3(s)+Li_2O(s)\}$ phase mixture was used for further calculation and is expressed as

$$\ln(K_{inst}) = 3711.9/(T/K) - 47.05 \quad (614 \le T/K \le 750) \tag{6}$$

3.2.1. Phase mixture $\{2LiFe_5O_8(s)+Li_2CO_3(s)+5Fe_2O_3(s)\}$

The ion intensities of CO_2^+ as a function of temperature over $\{LiFe_5O_8(s)+Li_2CO_3(s)+5Fe_2O_3(s)\}$ were measured in the temperature range 588–761 K. Partial pressure of CO_2(g), $p(CO_2)$, at different temperatures for two different runs were calculated using the measured ion intensities and Eqs. (5) and (6) and tabulated in Table 1. The variation of logarithmic values of $p(CO_2)$ as a function of reciprocal of temperature follows linear relationship as shown in Fig. 5 and can be expressed as

$$\ln\{p(CO_2/atm)\} = -22492(\pm989)/(T/K) + 17.56(\pm1.5) \quad (588 \le T/K \le 761) \tag{7}$$

Table 1
Partial pressure of CO_2(g) over ternary phase mixtures.

$\{2LiFe_5O_8(s)+Li_2CO_3(s)+5Fe_2O_3(s)\}$			$\{2LiFeO_2(s)+Li_2CO_3(s)+Fe_2O_3(s)\}$		
***T* (K)**	***I* (A)**	***p*(CO_2) (atm)**	***T* (K)**	***I* (A)**	***p*(CO_2) (atm)**
1st run			***1st run***		
588	1.72E−13	2.432E−9	569	1.96E−13	2.682E−9
599	3.06E−13	4.408E−9	586	3.90E−13	5.496E−9
614	5.35E−13	7.899E−9	600	9.91E−13	1.430E−8
639	1.68E−12	2.581E−8	615	2.21E−12	3.268E−8
653	4.01E−12	6.297E−8	628	4.42E−12	6.675E−8
671	1.01E−11	1.630E−7	636	6.96E−12	1.064E−7
678	1.59E−11	2.592E−7	646	1.06E−11	1.647E−7
689	2.82E−11	4.672E−7	656	1.86E−11	2.934E−7
700	5.12E−11	8.618E−7	667	3.11E−11	4.988E−7
710	8.03E−11	1.371E−6	675	5.36E−11	8.700E−7
719	1.24E−10	2.144E−6	686	9.75E−11	1.608E−6
729	1.92E−10	3.366E−6	695	1.49E−10	2.490E−6
740	3.03E−10	5.392E−6	706	2.65E−10	4.499E−6
2nd run			***2nd run***		
607	1.92E−13	2.803E−9	591	4.65E−13	6.608E−9
622	3.67E−13	5.489E−9	605	8.44E−13	1.228E−8
634	5.45E−13	8.309E−9	621	2.00E−12	2.987E−8
643	8.26E−13	1.277E−8	636	4.21E−12	6.439E−8
659	1.88E−12	2.979E−8	641	5.84E−12	9.002E−8
665	2.37E−12	3.790E−8	652	9.71E−12	1.522E−7
675	4.22E−12	6.850E−8	662	1.63E−11	2.595E−7
685	7.52E−12	1.239E−7	672	2.62E−11	4.234E−7
694	1.20E−11	2.003E−7	678	4.07E−11	6.636E−7
704	2.08E−11	3.521E−7	690	8.11E−11	1.346E−6
714	3.97E−11	6.816E−7	701	1.40E−10	2.360E−6
724	6.16E−11	1.072E−6	711	2.71E−10	4.633E−6
735	1.07E−10	1.891E−6			
738	1.20E−10	2.130E−6			
748	1.97E−10	3.543E−6			
761	3.30E−10	6.039E−6			

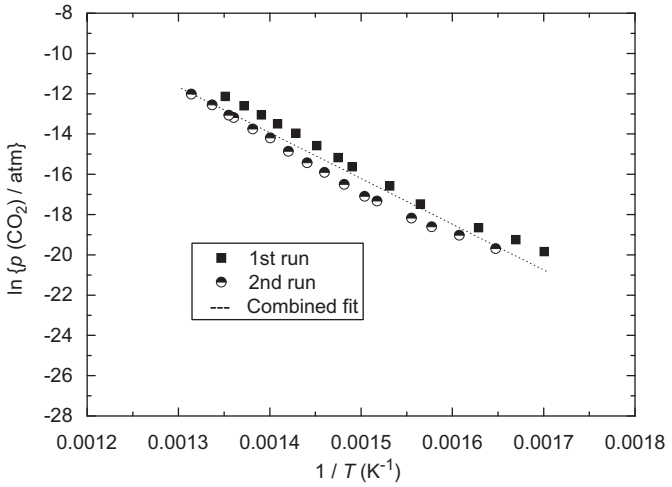

Fig. 5. Variation of $p(CO_2)$ as a function of temperature over $\{2LiFe_5O_8(s)+Li_2CO_3(s)+Fe_2O_3(s)\}$ phase mixture.

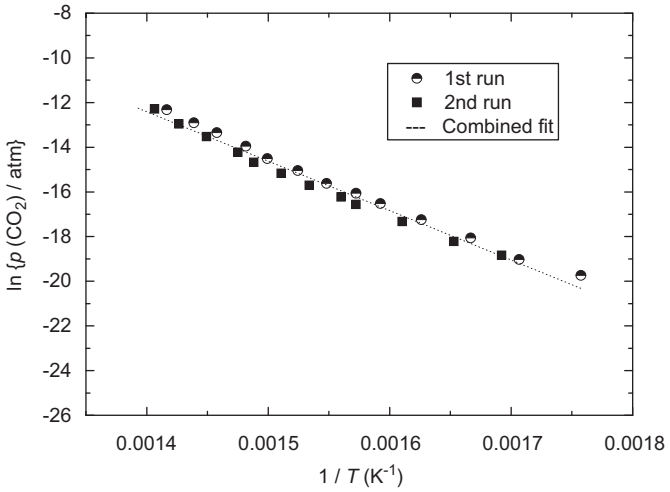

Fig. 6. Variation of $p(CO_2)$ as a function of temperature over $\{2LiFeO_2(s)+Li_2CO_3(s)+Fe_2O_3(s)\}$ phase mixture.

Table 2
Standard molar Gibbs energy of formation, $\Delta_f G^o_m(T)$, of different compounds used for calculation in this study.

Compound	$\Delta_f G^o_m(T)$ (kJ mol^{-1}) [19] (700–1200 K)
CO_2(g)	−394–0.0019(T/K)
Li_2CO_3(s)	−1213+0.2819(T/K)
Fe_2O_3(s)	−813+0.2543(T/K)
MgO(s)	−608+0.1151(T/K)
MgF_2(s)	−1124+0.1729(T/K)
CaF_2(s)	−1219+0.1618(T/K)
CaO(s)	−637+0.1065(T/K)
LiF(s)	−619+0.0973(T/K)

The enthalpy changes due to reaction (3) at the average temperature of measurement was found to be $\Delta_r H^o_m(675\,K) = (187 \pm 8)$ kJ mol^{-1}. The standard Gibbs energy for reaction (3) is calculated as

$$\Delta_{r(3)} G^o_m(T)/kJ\,mol^{-1}(\pm 8) = 187 - 0.146(T/K) \quad (588 \le T/K \le 761) \tag{8}$$

The standard molar Gibbs energies of formation ($\Delta_f G^o_m$) of $LiFe_5O_8$(s) from the elements were calculated from Eqs. (3) and (8) and the values of $\Delta_f G^o_m(T)$ for CO_2(g), Li_2CO_3(s) and Fe_2O_3(s) from Table 2 and is expressed as

$$\Delta_f G^o_m(LiFe_5O_8,s,T)/kJ\,mol^{-1}(\pm 8) = -2348 + 0.6881(T/K)$$
$$(588 \le T/K \le 761) \tag{9}$$

3.2.2. Phase mixture {2LiFeO$_2$(s)+Li$_2$CO$_3$(s)+Fe$_2$O$_3$(s)}

The ion intensities of CO_2^+ as a function of temperature over the above phase mixture were measured in the temperature range 569–711 K. Partial pressure of CO_2(g) at different temperatures for two different runs were calculated using the measured ion intensities and Eqs. (5) and (6) and tabulated in Table 1. The variation of logarithmic values of $p(CO_2)$ as a function of reciprocal of temperature follows linear relationship as shown in Fig. 6 and can be expressed as

$$\ln\{p(CO_2/atm)\} = -22089(\pm 570)/(T/K) + 18.56(\pm 0.9)$$
$$(569 \le T/K \le 711) \tag{10}$$

The enthalpy changes due to reaction (4) at the average temperature of measurement was found to be $\Delta_r H^o_m(640\,K) = (184 \pm 5)$ kJ mol^{-1}. The standard molar Gibbs energy of reaction (4) is calculated as

$$\Delta_{r(4)} G^o_m(T)/kJ\,mol^{-1}(\pm 5) = 184 - 0.1543(T/K)$$
$$(569 \le T/K \le 711) \tag{11}$$

The standard molar Gibbs energies of formation ($\Delta_f G^o_m$) of $LiFeO_2$(s) from the elements were calculated from Eqs. (4) and (11) and the values of $\Delta_f G^o_m(T)$ for CO_2(g), Li_2CO_3(s) and Fe_2O_3(s) from Table 2 and is expressed as

$$\Delta_f G^o_m(LiFeO_2,s,T)/kJ\,mol^{-1}(\pm 5) = -724 + 0.1919(T/K)$$
$$(569 \le T/K \le 711) \tag{12}$$

3.3. Emf measurements on cells (1), (2) and (3) using solid-state galvanic cell technique

3.3.1. Standardization of solid-state galvanic cell using cell (1)

The reversible emf values obtained at different experimental temperatures for cell (1) are listed in Table 3 and the variation of emf with temperature is shown in Fig. 7. The emf data were least squares fitted to yield the following linear relation:

$$E/V(\pm 0.0002) = 0.3956 - 2.1073 \times 10^{-5}(T/K)$$
$$(921 \le T/K \le 1150) \tag{13}$$

Table 3
Variation of emf as a function of temperature for cells (1), (2) and (3).

Cell (1)		Cell (2)		Cell (3)	
T (K)	E (V)	T (K)	E (V)	T (K)	E (V)
921	0.3762	808	0.0220	907	0.0132
941	0.3758	828	0.0227	927	0.0159
960	0.3754	842	0.0245	947	0.0184
982	0.3749	857	0.0265	960	0.0204
1000	0.3746	877	0.0276	966	0.0219
1019	0.3741	895	0.0303	975	0.0223
1042	0.3736	913	0.0305	984	0.0247
1060	0.3733	934	0.0323	1002	0.0257
1072	0.3730	953	0.0332	1012	0.0263
1088	0.3727	967	0.0339	1021	0.0270
1101	0.3724	971	0.0358		
1122	0.3720				
1134	0.3717				
1150	0.3714				

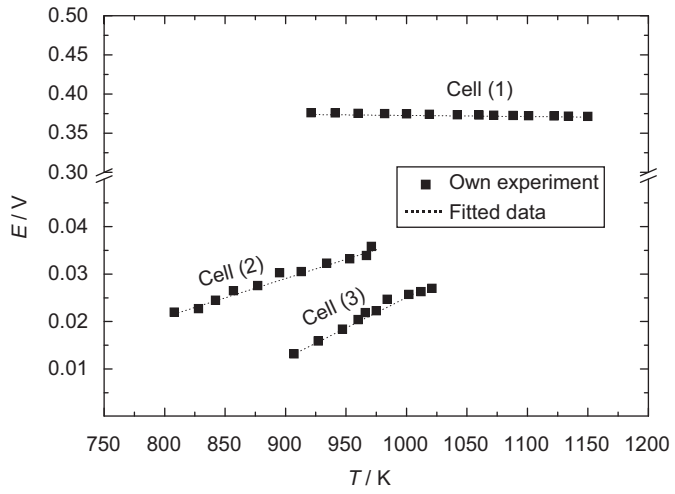

Fig. 7. Variation of emf as a function of temperature for cells (1), (2) and (3).

The half-cell reactions at each electrode can be represented as

$$MgF_2(s)+2e^-+\tfrac{1}{2}O_2(g)=MgO(s)+2F^- \quad (\text{at } +\text{ve electrode}) \tag{14}$$

and

$$CaO(s)+2F^-=CaF_2(s)+2e^-+\tfrac{1}{2}O_2(g) \quad (\text{at } -\text{ve electrode}) \tag{15}$$

The net virtual cell reaction can be represented as

$$MgF_2(s)+CaO(s)=CaF_2(g)+MgO(s) \tag{16}$$

The Gibbs energy change for the net cell reaction is calculated from the general relation

$$\Delta_r G^o=-nFE \tag{17}$$

where '*n*' is the total number of electrons involved in the half-cell reactions and '*F*' is the Faraday's constant ($F=96486.4\ C\ mol^{-1}$) and '*E*' is the net cell emf in volts. The values of $\Delta_{r(16)}G^o(T)$ as a function of temperature can be calculated using Eqs. (13) and (17) ($n=2$) and is represented by the following expression:

$$\Delta_{r(16)}G^o(T)/kJ\,mol^{-1}(\pm 0.1)=-76.3+0.0041(T/K) \quad (921\le T/K\le 1150) \tag{18}$$

The values of $\Delta_{r(16)}G^o(T)$ obtained in this study are in good agreement ($\pm 2.0\ kJ\ mol^{-1}$) with those calculated using the values of standard molar Gibbs energy of formations for $CaF_2(s)$, $MgF_2(s)$, MgO(s) and CaO(s) from Table 2.

3.3.2. $\Delta_f G^o(T)$ for $LiFe_5O_8(s)$ using emf studies on cell (2)

The reversible emf values obtained at different temperatures from 808–971 K for cell (2) are listed in Table 3 and the variation of emf with temperature is shown in Fig. 7. The emf data were least squares fitted to yield the following linear relation:

$$E/V(\pm 0.0007)=-0.0435+8.1048\times 10^{-5}(T/K) \quad (808\le T/K\le 971) \tag{19}$$

The half-cell reactions at each electrode can be represented as

$$2LiF(s)+5Fe_2O_3(s)+\tfrac{1}{2}O_2(g)+2e^-=2LiFe_5O_8(s)+2F^- \quad (\text{at } +\text{ve electrode}) \tag{20}$$

and

$$CaO(s)+2F^-=CaF_2(s)+\tfrac{1}{2}O_2(g)+2e^- \quad (\text{at } -\text{ve electrode}) \tag{21}$$

The net virtual cell reaction can be represented as

$$LiF(s)+5Fe_2O_3(s)+CaO(s)=2\ LiFe_5O_8(s)+CaF_2(s) \tag{22}$$

The Gibbs energy change for the net cell reaction was calculated from the general relation (17) ($n=2$) and Eq. (19) and is expressed as

$$\Delta_{r(22)}G^o(T)/kJ\,mol^{-1}(\pm 0.1)=8.4-0.0156(T/K) \quad (808\le T/K\le 971) \tag{23}$$

The standard molar Gibbs energy of formation, $\Delta_f G^o_m(T)$ of $LiFe_5O_8(s)$ was obtained by using Eqs. (22) and (23) and the values of $\Delta_f G^o_m(T)$ for $Fe_2O_3(s)$, CaO(s), LiF(s) and $CaF_2(s)$ from Table 2

$$\Delta_f G^o_m(T)/kJ\,mol^{-1}(\pm 0.7)=-2345+0.6811(T/K) \quad (808\le T/K\le 971) \tag{24}$$

The temperature independent term of the above Eq. (24) represents $\Delta_f H^o_m(T_{av}=890\ K)$ and temperature dependent term represents negative change in entropy of $LiFe_5O_8(s)$.

3.3.3. $\Delta_f G^o(T)$ for $LiFeO_2(s)$ using emf studies on cell (3)

The reversible emf values obtained at different temperatures from 907–1021 K for cell (3) are listed in Table 3 and the variation of emf with temperature is shown in Fig. 7. The emf data were least squares fitted to yield the following linear relation:

$$E/V(\pm 0.006)=-0.0997+1.2504\times 10^{-4}(T/K)(907\le T/K\le 1021) \tag{25}$$

The half-cell reactions at each electrode can be represented as

$$4LiF(s)+LiFe_5O_8(s)+O_2(g)+4e^-=5LiFeO_2(s)+4F^- \quad (\text{at } +\text{ve electrode}) \tag{26}$$

and

$$2CaO(s)+4F^-=2CaF_2(s)+O_2(g)+4e^- \quad (\text{at } -\text{ve electrode}) \tag{27}$$

The net virtual cell reaction can be represented as

$$4LiF(s)+LiFe_5O_8(s)+2CaO(s)=5LiFeO_2(s)+2CaF_2(s) \tag{28}$$

The Gibbs energy change for the net cell reaction (28) was calculated from the general relation (17) ($n=4$) and Eq. (25) and is expressed as

$$\Delta_{r(28)}G^o(T)/kJ\,mol^{-1}(\pm 2.3)=38.5-0.0482(T/K) \quad (907\le T/K\le 1021) \tag{29}$$

The standard molar Gibbs energy of formation, $\Delta_f G^o_m(T)$ of $LiFeO_2(s)$ was obtained using Eqs. (28) and (29) and the values of $\Delta_f G^o_m(T)$ for $LiFe_5O_8(s)$ from Eq. (24) and that of CaO(s), LiF(s) and $CaF_2(s)$ from Table 2

$$\Delta_f G^o_m(T)/kJ\,mol^{-1}(\pm 2.3)=-724+0.1823(T/K) \quad (907\le T/K\le 1021) \tag{30}$$

The temperature independent term of the above Eq. (30) represents $\Delta_f H^o_m(T_{av}=964\ K)$ and temperature dependent term represents negative change in entropy of $LiFeO_2(s)$.

3.4. Comparison of $\Delta_f G^o(T)$ of $LiFe_5O_8(s)$ and $LiFeO_2(s)$ using KEQMS and emf studies

Fig. 8 shows the plot of $\Delta_f G^o_m(T)$ for $LiFe_5O_8(s)$ and $LiFeO_2(s)$ as a fucntion of temperature determined from KEQMS and emf techniques along with literature values. The figure shows that the values of $\Delta_f G^o_m(T)$ determined from two different experiements are in close agreement. Hence, these two sets of data are combined to generate the Gibbs energy as a function of temperature in a wide temperature range covering both the experimental techniques. The combined data for both the compounds are least squares fitted and the expressions are given below:

$$\Delta_f G^o_m(LiFe_5O_8,s,T)/kJ\,mol^{-1}(\pm 6)=-2341+0.6764(T/K) \quad (588\le T/K\le 971) \tag{31}$$

$$\Delta_f G^o_m(LiFeO_2,s,T)/kJ\,mol^{-1}(\pm 3) = -708 + 0.1656(T/K) \quad (569 \le T/K \le 1021) \tag{32}$$

The temperature independent term of the above equations represents $\Delta_f H^o_m(T_{av})$ and temperature dependent term represents negative change in entropy $\{-\Delta_f S^o_m(T_{av})\}$ of respective compounds. Kawamura et al. [16] have reported the $\Delta_f G^o_m(T)$ for $LiFeO_2$(s) from 673 to 873 K using galvanic cell experiments which are expressed as

$$\Delta_f G^o_m(LiFeO_2,s,T)/kJ\,mol^{-1} = -752 + 0.187(T/K) \quad (673 \le T/K \le 873) \tag{33}$$

These $\Delta_f G^o_m(T)$ values have been compared with this study in Fig. 8 and found that the values are 20–30 kJ more negative compared to this study.

3.5. Second law analysis of experimental data

Second law analysis was carried out to calculate $\Delta_f H^o_m$(298.15 K) and S^o_m(298.15 K) for $LiFe_5O_8$(s) and $LiFeO_2$(s) using heat capacity data and standard molar Gibbs energy of formation of these compounds from Eqs. (31) and (32) and auxiliary data of Li(s, l), Fe(s) and O_2(g) from literature [19]. The corresponding data are listed in Table 4. Several authors have reported the $\Delta_f G^o_m(T)$, $\Delta_f H^o_m(T)$ and S^o_m(298) for $LiFe_5O_8$(s) and $LiFeO_2$(s) [13–17,29]. These values are compared in Table 4 along with data of the present study. It is observed that $\Delta_f H^o_m$(298 K) value calculated by Berbenni et al. [29] for $LiFe_5O_8$(s) is 61 kJ more negative compared to this study. In case of $LiFeO_2$(s), small deviations were observed in thermochemical data among various researchers [13–17].

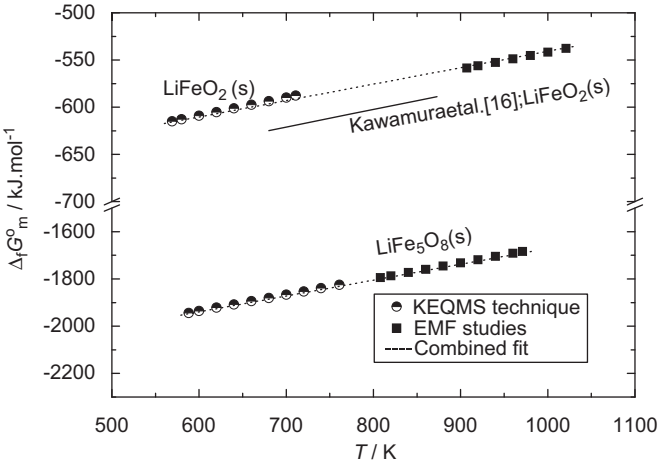

Fig. 8. Comparison of $\Delta_f G^o_m(T)$ of lithium ferrites determined using different techniques.

3.6. Construction of thermodynamic table for $LiFe_5O_8$(s) and $LiFeO_2$(s)

Thermodynamic table includes the basic functions such as: $\Delta_f H^o_m$(298.15 K), $S^o_m(T)$, $C^o_{p,\,m}(T)$, $\{H^o_m(T)-H^o_m(298.15\ K\}$, $G^o_m(T)$, $\Delta_f H^o_m(T)$, $\Delta_f G^o_m(T)$ and free energy function (*fef*). These functions were calculated using the thermodynamic data obtained in the present study using 'FactSage' software [30]. The molar heat capacity values of Li(s, l), Fe(s) and O_2(g) required for the second law analysis have been taken from 'FactSage' thermochemical database software and experimental heat capacity values of $LiFe_5O_8$(s) and $LiFeO_2$(s) were extrapolated to 1000 K and thermodynamic values of the most stable phases were used.

For the compound $LiFe_5O_8$(s), Yang et al. [31] has reported a magnetic order-disorder transition in the temperature range of 863–923 K which depends on the particle size ranging from 9.1 to 860 nm. This suggests that the magnetic transition present in $LiFe_5O_8$(s) is highly dependent on its particle size. Since, in this study we have not observed any transition either in the heat capacity measurement or in emf experiment for our sample; hence construction of thermodynamic table was carried out assuming there is no transition in $LiFe_5O_8$(s).

After calculation of all the thermodynamic fucntions, the values obtained at selected temepratures from 298 to 1000 K are tabulated and are given in Tables 5 and 6 for $LiFe_5O_8$(s) and $LiFeO_2$(s), respectively.

Further, the values of $\Delta_r H^o_m$(298.15 K) for the reactions (3) and (4) were calculated using third law analysis and experimental $p(CO_2)$ values from KEQMS experiments. These values were plotted as a function of experimental temperature and are shown in Fig. 9 which do not reveal any systematic trend in the values of $\Delta_r H^o_m$(298.15 K) for these reactions.

3.7. Comparison of thermodynamic stabilities of $LiFe_5O_8$(s) and $LiFeO_2$(s)

The Gibbs energy of mixing (ΔG^M_m) of compound is a very good tool to compare the relative stabilities of double oxides. The values of ΔG^M_m are obtained by dividing the standard molar Gibbs energies of

Table 4
Thermochemical data for lithium ferrites.

Compound	Thermochemical data		T (K)	Method and references
	$\Delta_f H^o_m$ (kJ mol^{-1})	S^o_m (J K^{-1} mol^{-1})		
$LiFe_5O_8$(s)	−2370	244.6	298	KEQMS, 2nd law, this study
	−2371	247.1	298	KEQMS, 3rd law, this study
	−2387	226.4	298	Galvanic cell, this study
	−2373	243.0	298	Combined, 2nd law, this study
	−2434	–	298	Calculated from reaction enthalpy [29]
$LiFeO_2$(s)	−731	73.8	298	KEQMS, 2nd law, this study
	−729	72.3	298	KEQMS, 3rd law, this study
	−736	75.9	298	Galvanic cell, this study
	−719	75.8	298	Combined, 2nd law, this study
	−750	–	298	Drop solution calorimetry [13]
	$\Delta_f G^o_m = -694$	–	298	Estimated [13]
	$\Delta_f G^o_m = -645$	–	673	Electrochemical [14]
	$\Delta_f G^o_m = -694$	–	300	Chemical potential [15]
	$\Delta_f G^o_m = -752 + 0.187\ (T/K)$	–	673–873	Galvanic cell [16]
	–	75.3	298	Heat capacity measurement [17]

Table 5
Thermodynamic functions for the compound $LiFe_5O_8$(s).

T (K)	C_p^o (J K^{-1} mol^{-1})	H^o (kJ mol^{-1})	G^o (kJ mol^{-1})	S^o (J K^{-1} mol^{-1})	$H_T^o - H_{298.15}^o$ (J mol^{-1})	fef (J K^{-1} mol^{-1})	$\Delta_f H^o$ (kJ mol^{-1})	$\Delta_f G^o$ (kJ mol^{-1})
298.15	298.1	−2373.0	−2445.5	243.0	0	243.0	−2373.0	−2151.6
300	298.9	−2372.4	−2445.9	244.8	552	243.0	−2372.9	−2150.2
350	318.9	−2356.9	−2459.4	292.5	16,011	246.7	−2371.0	−2113.2
400	336.2	−2340.6	−2475.1	336.2	32,395	255.2	−2368.6	−2076.6
450	351.9	−2323.4	−2492.9	376.7	49,604	266.5	−2365.8	−2040.2
500	366.7	−2305.4	−2512.7	414.5	67,575	279.4	−2365.7	−2003.9
550	380.9	−2286.7	−2534.3	450.2	86,270	293.3	−2362.3	−1967.9
600	394.7	−2267.3	−2557.7	483.9	105,662	307.8	−2358.5	−1932.2
650	408.1	−2247.3	−2582.7	516.1	125,734	322.6	−2354.6	−1896.8
700	421.4	−2226.5	−2609.3	546.8	146,473	337.5	−2350.4	−1861.8
750	434.5	−2205.1	−2637.4	576.3	167,870	352.5	−2346.1	−1827.0
800	447.4	−2183.1	−2666.9	604.7	189,916	367.4	−2341.7	−1792.6
850	460.3	−2160.4	−2697.8	632.3	212,608	382.1	−2337.4	−1758.4
900	473.0	−2137.1	−2730.1	658.9	235,941	396.8	−2333.2	−1724.4
950	485.8	−2113.1	−2763.7	684.8	259,911	411.3	−2329.3	−1690.7
1000	498.4	−2088.5	−2798.6	710.1	284,515	425.6	−2325.9	−1657.2

Table 6
Thermodynamic functions for the compound $LiFeO_2$(s).

T (K)	C_p^o (J K^{-1} mol^{-1})	H^o (kJ mol^{-1})	G^o (kJ mol^{-1})	S^o (J K^{-1} mol^{-1})	$H_T^o - H_{298.15}^o$ (J mol^{-1})	fef (J K^{-1} mol^{-1})	$\Delta_f H^o$ (kJ mol^{-1})	$\Delta_f G^o$ (kJ mol^{-1})
298.15	79.1	−719.0	−741.6	75.8	0	75.8	−719.0	−663.7
300	79.6	−718.9	−741.7	76.3	147	75.8	−718.9	−663.3
350	89.3	−714.6	−745.9	89.3	4384	76.8	−718.8	−654.1
400	96.1	−709.9	−750.7	101.7	9028	79.2	−718.3	−635.7
450	101.2	−705.0	−756.0	113.4	13,966	82.3	−717.7	−635.0
500	105.3	−699.8	−761.9	124.2	19,131	86.0	−720.0	−626.3
550	108.6	−694.5	−768.5	134.4	24,480	89.9	−719.2	−616.9
600	111.5	−689.0	−775.4	144.0	29,985	94.0	−718.4	−607.7
650	114.1	−683.4	−782.8	153.0	35,627	98.2	−717.4	−598.5
700	116.4	−677.6	−790.7	161.6	41,390	102.4	−716.5	−589.4
750	118.6	−671.7	−799.0	169.7	47,264	106.7	−715.5	−580.4
800	120.6	−665.8	−807.7	177.4	53,243	110.8	−714.6	−571.4
850	122.5	−659.7	−816.7	184.7	59,319	115.0	−713.6	−562.5
900	124.3	−653.5	−826.1	191.8	65,489	119.1	−712.8	−553.6
950	126.1	−647.3	−835.9	198.6	71,749	123.1	−712.1	−544.8
1000	127.8	−640.9	−846.0	205.1	78,095	127.0	−711.5	−536.0

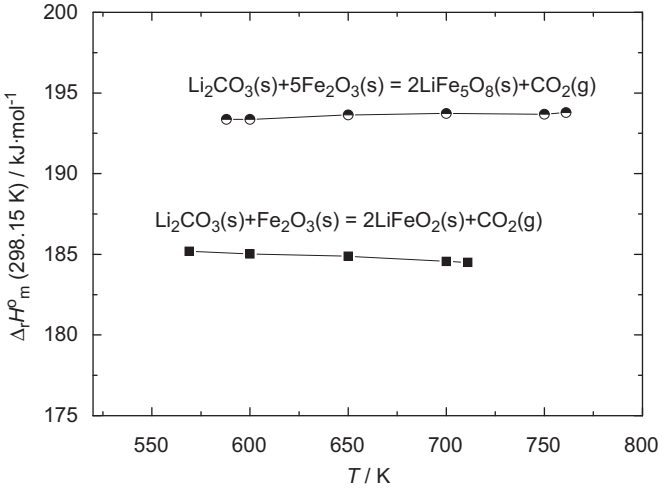

Fig. 9. Variation of $\Delta_r H_m^o(298\ K)$ of lithium ferrites determined from KEQMS technique using third law analysis.

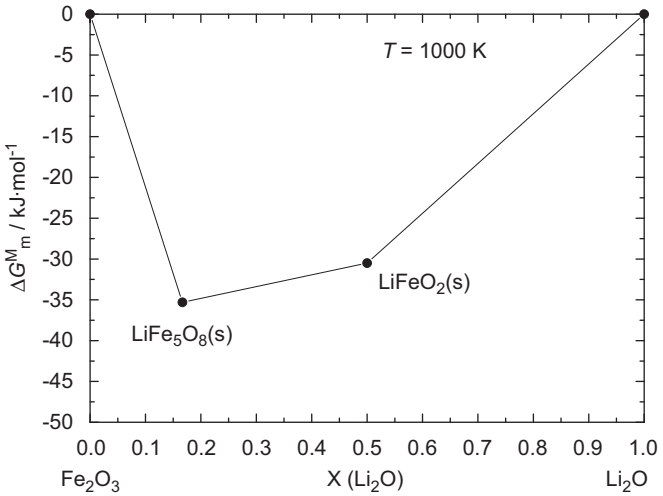

Fig. 10. Gibbs energy of mixing of lithium ferrites at 1000 K.

formation of ternary oxides from its component binary oxides by the number of molecules of the binary oxides present in the compound. These values were calculated for $LiFe_5O_8$(s) and $LiFeO_2$(s) at 1000 K and shown in Fig. 10, which shows that $LiFe_5O_8$(s) is relatively more stable compared to $LiFeO_2$(s).

4. Conclusions

The thermodynamic data of $LiFe_5O_8$(s) and $LiFeO_2$(s) have been generated using differential scanning calorimetry, Knudsen effusion quadrupole mass spectrometry and solid-state galvanic cell methods.

The experimental data are combined together by carrying out second law analysis and thermodynamic data table from 298.15 to 1000 K have been generated. Thermodynamic analysis show that $LiFe_5O_8$(s) is more stable compared to $LiFeO_2$(s). These data are valuable for predicting the thermodynamic stabilities of these compounds in different physico-chemical conditions.

References

[1] M.G.S.R. Thomas, W.I.F. David, J.B. Goodenough, P. Groves, Mater. Res. Bull. 20 (1985) 1137.
[2] J.R. Dahn, U. Von Sacken, C.A. Michal, Solid State Ionics 44 (1990) 87.
[3] Y. Sakurai, H. Arai, S. Okada, J. Yamaki, J. Power Sour. 68 (1997) 711.
[4] G.M. Argentina, P.D. Baba, IEEE Trans. Microwave Theory Tech. MTT-2 (1974)652 MTT-2 (1974).
[5] X. Qi, J. Zhou, Z. Yue, Z. Gui, L. Li, Mater. Sci. Eng. B 99 (2003) 278.
[6] Yen-Pei Fu, Cheng-Hsiung Lin, Chung-Wen Liu, Yeong-Der Yao, J. Alloys Compd. 395 (2005) 247.
[7] V. Berbenni, A. Marini, G. Bruni, R. Riccardi, Thermochim. Acta 346 (2000) 115.
[8] N. Ramachandran, A.B. Biswas, J. Solid State Chem. 30 (1979) 61.
[9] T. Shirane, R. Kanno, Y. Kawamoto, Y. Takeda, M. Takano, T. Kamiyama, F. Izumi, Solid State Ionics 79 (1995) 227.
[10] M. Tabuchi, K. Ado, H. Kobayashi, I. Matusubara, H. Kageyama, M. Wakita, S. Tsutsui, S. Nasu, Y. Takeda, C. Masquelier, A. Hirano, R. Kanno, J. Solid State Chem. 141 (1998) 554.
[11] K. Hashimoto, M. Nishikawa, N. Nakashima, S. Beloglazov, M. Enoeda, Fusion Eng. Des. 61–62 (2002) 375.
[12] W. Heyi, Z. Jumke, L. Yangming, J. Nucl. Mater. 208 (1994) 195.
[13] M. Wang, A. Navrotsky, J. Solid State Chem. 178 (2005) 1230.
[14] N.A. Godshall, I.D. Raistrick, R.A. Huggins, J. Electrochem. Soc. 131 (1984) 543.
[15] H. Yokokawa, N. Sakai, K. Yamaji, T. Horita, M. Ishikawa, Solid State Ionics 113–115 (1998) 1.
[16] H. Kawamura, K. Asano, S. Nagano, A. Kaimai, K. Yashiro, Y. Nigara, T. Kawada, J. Mizusaki, Ionic and mixed conducting ceramics IV, in: T.A. Ramanarayanan (Ed.), Proceedings of the Fourth International Symposium, The Electrochemical Society, Inc., Pennington, NJ, 2002, p. 272.
[17] E.G. King, J. Am. Chem. Soc. 77 (1955) 3189.
[18] S.K. Rakshit, S.C. Parida, S. Dash, Z. Singh, B.K. Sen, V. Venugopal, J. Solid State Chem. 180 (2007) 523.
[19] M.W. Chase Jr., JANAF Thermochemical Tables, 4th ed., J. Phys. Chem. Ref. Data, Monograph No. 9, 1995.
[20] G.A. Murray, R.A. Kematick, C.E. Myers, High Temp. Sci. 26 (1990) 4.
[21] V.L. Stolyarova, D.U. Sichen, S. Seetharaman, Vacuum 46 (8–10) (1995) 871.
[22] J.A. Basford, M.D. Boeckmann, R.E. Ellefson, A.R. Filippelli, D.H. Holkeboer, L. Lieszkovszky, C.M. Stupak, J. Vac. Sci. Technol. A 11 (3) (1993) A22.
[23] M.C. Cowen, W. Allison, J.H. Batey, J. Vac. Sci. Technol. A 12 (1) (1994) 228.
[24] M.G. Rao, C. Dong, J. Vac. Sci. Technol. A 15 (3) (1997) 1312.
[25] S.K. Rakshit, Y.P. Naik, S.C. Parida, Smruti Dash, Ziley Singh, B.K. Sen, V. Venugopal, J. Solid State Chem. 181 (2008) 1402.
[26] J. Huang, T. Furkawa, K. Aoto, J. Chem. Thermodyn. 38 (2006) 1.
[27] I. Barin, 3rd ed., Thermochemical Data of Pure Substances, vols. I & II, VCH Publishers, New York, 1995.
[28] J.B. Mann, J. Chem. Phys. 46 (1967) 1646.
[29] V. Berbenni, A. Marini, D. Capsoni, Z. Naturforsch. 53A (1998) 997.
[30] FactSage version 5.3.1., Thermo-chemical database, Thermfact, GTT Technologies, Germany, 1976–2004.
[31] Hua Yang, Zichen Wang, Muyu Zhao, Jianping Wang, Dehua Han, Helie Luo, Li Wang, Mater. Chem. Phys. 48 (1997) 60.